

Effects of Image Charges on the Scavenging of Aerosol Particles by Cloud Droplets and on Droplet Charging and Possible Ice Nucleation Processes

B. A. TINSLEY, R. P. ROHRBAUGH, AND M. HEI

William B. Hanson Center for Space Sciences, University of Texas at Dallas, Richardson, Texas

K. V. BEARD

University of Illinois, Urbana-Champaign, Urbana, Illinois

(Manuscript received 20 November 1998, in final form 20 August 1999)

ABSTRACT

Previous calculations of the rate at which falling droplets in clouds collide with aerosols have led to the conclusion that except in thunderclouds any electrical charges on the aerosols or droplets have little effect on the collision rate. However, it had been assumed that the aerosols would have only a few elementary charges on them, whereas it is now known that at the tops of nonthunderstorm clouds the evaporating droplets may have several hundred elementary charges on them and that much of this charge remains on the residual aerosol for 5 min or so after the evaporation. Also, most previous calculations neglected image charge forces that provide strong attraction at close range even when droplet and aerosol have charges of the same sign and of comparable magnitude.

The authors present numerical calculations showing that electrical effects dominate collision rates for charged evaporation aerosols. The calculations are for the size range of 0.1- to 1.0- μm radius with the collision efficiency compared to that for phoretic and Brownian effects being greater by up to a factor of 30 greater for droplets from 18.6- to 106- μm radius with relative humidity in the range 95%–100% and only 50 elementary charges on the aerosol. The results imply that electrical effects can be important for the scavenging of evaporation aerosol particles in the size range of the Greenfield gap.

The authors call this process “electroscavenging.” Electroscavenging of charged particles, when the particles are mostly of the same sign, is a previously unrecognized droplet charging process. Electroscavenging also provides a pathway for contact ice nucleation when charged aerosol particles from evaporated charged droplets collide with supercooled droplets. Ice nucleation can occur because aerosol particles from the evaporation of cloud droplets have been found to be more effective as ice forming nuclei than other aerosol particles that have not been processed through droplets.

1. Introduction

Calculations of the collision efficiency for aerosol particles in the path of falling water droplets have been reviewed by Pruppacher and Klett (1997, section 18.6.6). Collision efficiency is defined as the fraction of the particles in the cylindrical volume swept out by a falling droplet that makes contact with the droplet. The tendency for particles in the range of radii 0.001–10 μm to be carried around the droplet by the flow, instead of making contact with it, results in collision efficiencies considerably less than unity. The collision efficiencies are less than 10^{-3} for aerosol particles of

radius 0.1–1.0 μm when in the path of droplets of radii a few tens of μm . At the low end of this aerosol particle size range the probability of collision is larger because of increasing amplitude of Brownian motion of the particle. At the upper end it is larger because of the increasing inertia of the particle that resists the tendency to be carried by the stream flow around the droplet. The region of low collision efficiency in the middle is known as the Greenfield Gap, following the work of Greenfield (1957), and in this region the collision efficiencies are susceptible to enhancement by electrical and other effects.

Numerical calculations of electric charge effects on particle–droplet collisions were made by Grover and Beard (1975), who considered 38 cases of various charges on 42- and 142- μm radius droplets and 0.4- and 4.0- μm radius particles. They found significant increases in collision efficiency, for charges of thunderstorm mag-

Corresponding author address: B. A. Tinsley, MS FO 22, University of Texas at Dallas, P.O. Box 830688, Richardson, TX 75083-0688.
E-mail: tinsley@utdallas.edu

nitude ($>7 \times 10^4$ elementary charges) on droplets, with charges on the particles of opposite sign. The particle charges assumed were generally greater in magnitude than for charged particles in Boltzman equilibrium with bipolar ions (see section 4). Calculations were made for the droplets and particles assumed to be conducting spheres (i.e., image charges taken into account) and alternatively for point charges at the centers of nonconducting spheres. Two of the cases considered were for 42- μm droplets and 0.4- μm particles treated as conducting spheres with zero charge on the droplets and 67 and 6.7 elementary charges on the particles. The present results are in reasonable agreement with these two cases as will be discussed in section 3.

Comprehensive numerical calculations were made by Wang et al. (1978) and were based on the assumption that the droplet and the particle had charges of opposite sign and that the electrical force between them was due to point charges at the particle centers. Also, the relative amounts of charge on the particle and droplet were considered to be proportional to the square of their radii so the droplet charge was always much greater than the particle charge. Modest increases in collision rate were found in the Greenfield gap provided that there were thousands of elementary charges on the droplet. This droplet charge is of the order of magnitude produced in thunderstorms. The charge (of opposite sign) on typical aerosol particles in the Greenfield Gap ranged from less than 1 to more than 40 elementary charges, again being generally greater than the average charge found on particles when ion diffusion in the atmosphere charges them to the Boltzman equilibrium charge levels. The implications that were drawn from these and other results were that for clouds in the atmosphere that were not electrified by thunderstorm processes, the effect of electrical forces on particle–droplet collisions would be insignificant.

The situation is different, however, for aerosol particles resulting from evaporation of charged droplets (Beard 1992). Nonthunderstorm clouds often include droplets with several hundred elementary charges on them (Pruppacher and Klett 1997, Fig. 18.1), and when such droplets evaporate little charge is removed. Thus, particles with several hundred elementary charges are produced. This charge is lost only slowly by conduction on a timescale of 10^2 – 10^3 s, partly because the conductivity within clouds is considerably less than that outside, as will be discussed in section 5. In this situation, where the particle charge is not extremely small compared to any droplet charge, the attractive force due to the generation on the droplet of an image charge of opposite sign can no longer be neglected. When evaporation occurs in downdrafts and there is a distribution of drop sizes in the parcel, the evaporation of the smaller droplets will occur with the air remaining close to 100% relative humidity (RH). Evaporation also occurs due to mixing at the cloud–dry air interface. As the smaller droplets evaporate down to haze particle size, or dry

aerosol particle size, they stop falling, while the remaining larger droplets continue to fall and approach them. As the separation becomes only a fraction of the droplet radius, the attractive force between the aerosol particle and its image on the droplet increases rapidly. Even in the case where there is net charge on the droplet that is of the same sign as that on the particle and therefore causes repulsion at a relatively long range, the image charge force can become great enough at short range to overcome it and ensure a collision when the motion of the droplet reduces the separation faster than the particle can recede.

Thus for droplets with a net charge that is zero, or of the same sign, or of opposite sign to that on the particle, the electrical effects due to image charges can dominate collision efficiencies. As we will show, this can occur even if much of the initial particle charge has leaked away and only tens of elementary charges remain on it. We call this process electroscavenging.

Electroscavenging is applicable to the atmosphere in the situation (Beard 1992) where charged droplets are evaporating and producing charged “evaporation” aerosol particles, that is, evaporation nuclei, which are thought to be effective ice-forming nuclei (Rosinski and Morgan 1991; Rosinski 1995). These charged evaporation nuclei may then undergo collisions with incompletely evaporated supercooled droplets and act as contact ice nuclei. The results are thus applicable to the modeling of ice nucleation processes and to the problem of accounting for the unexpectedly high ice particle concentrations in many clouds (see for example Hobbs and Rangno 1985; Beard 1992).

Electroscavenging is also applicable to the process of scavenging of radioactive aerosol particles. These become charged because of emissions of ions or electrons (Rosinski et al. 1962; Clement and Harrison 1992).

2. Theory for image charge effects on collision efficiency

Figures 1a and 1b illustrate the flow of aerosol particles around a falling droplet with and without electrical forces, and Figs. 1c and 1d define the relevant geometry. The origin of coordinates is taken at the droplet center, so that the droplet is stationary, with the air flowing upwards past the droplet. The electrical forces always act along the line of centers of the particle and droplet. The particle is taken as a point and the droplet is taken as a conducting sphere, undistorted by the electrical forces or by the airstream. The effects of Brownian motion and inertia and thermophoresis and diffusophoresis have been accurately evaluated in prior work (Wang et al. 1978; Pruppacher and Klett 1997, section 18.6.6), and in the present calculations we will consider that only electrical forces are moving the particle relative to the flow. The net phoretic force usually increases the collision efficiency when droplets are evaporating, that is, when the relative humidity is less than 100%. We

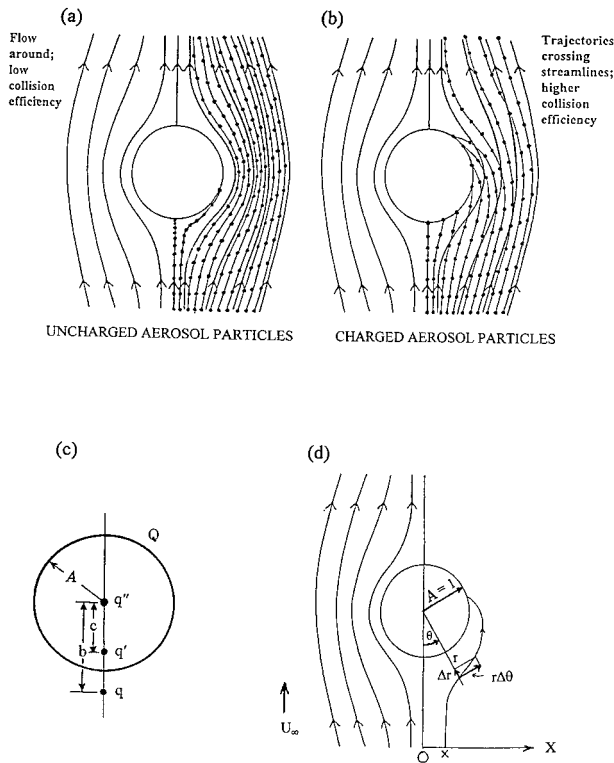


FIG. 1. (a) Schematic of aerosol flow around a falling droplet in the absence of electrical forces. (b) Schematic of the effect of electrical image forces on aerosol flow. (c) Location of aerosol particle and its image charge on a droplet of radius A . (d) Polar coordinate system used for numerical integration of particle trajectories.

will compare the magnitudes of the electrical effects with the magnitudes of the nonelectrical effects calculated by previous workers.

In Fig. 1c the droplet of radius A has a net charge Q , and the aerosol particle has a charge q and is at a distance b from the origin. It can be shown from the theory of electrostatics (e.g., Jackson 1975) that the particle charge causes the charge on the conducting droplet to redistribute itself, to be equivalent to two point charges. One is the image charge q' of amount $q' = -(A/b)q$, located on the line of centers at a distance c from the origin, plus the second, which is a point charge q'' at the droplet center, such that $Q = q' + q''$. The distance c is given by $c = A^2/b$. The conductivity of the droplet need not be large; only large enough so that the electrical relaxation time is small compared to the time for a significant change in spacing between particle and droplet. This is usually the case (Davis 1969).

Adding together the forces between the point charges in Fig. 1c, the total electrical force between droplet and particle is

$$F = \frac{qq'}{4\pi\epsilon_0(b-c)^2} + \frac{qq''}{4\pi\epsilon_0b^2}, \quad (1)$$

where a positive F is repulsive. Substituting for q' and q'' and c we obtain

$$F = \frac{q^2}{4\pi\epsilon_0} \left[-\frac{A/b}{(b-A^2/b)^2} + \frac{A}{b^3} \left(\frac{Qb}{qA} + 1 \right) \right], \quad (2)$$

that is,

$$F = \frac{q^2}{4\pi\epsilon_0A^2} \left[-\frac{b/A}{(b^2/A^2-1)^2} + \frac{A^3}{b^3} \left(\frac{Qb}{qA} + 1 \right) \right]. \quad (3)$$

In Fig. 1d the geometry necessary for evaluating the motion of the particle under the combined effects of flow and the net electric force is illustrated. It is convenient to normalize the calculation to that for a droplet of unit radius, so that the normalized distance of the particle is $r = b/A$. We define $C = q^2/(4\pi\epsilon_0A^2)$ and $K = Q/q$, so that

$$F = C \left[-\frac{r}{(r^2-1)^2} + \frac{1}{r^3}(Kr+1) \right]. \quad (4)$$

We define the term in square brackets as P , so that $F = CP$.

In Figs. 1a, 1b, and 1d the terminal fall velocity of the droplet is reflected in the upward stream velocity of asymptotic magnitude U_∞ . In the atmosphere U_∞ depends on the weight of the droplet and on the viscosity of the air. To determine the trajectory of the aerosol particle it is necessary to solve numerically the equations of fluid flow around the spherical droplet with the addition of the motion of the particle across streamlines due to the net electrical force F . We define the polar angle θ as being zero in the downward (upstream) direction and the radial velocity $u_r = \Delta r/\Delta t$ as being positive in the outward direction with the tangential velocity $u_\theta = r\Delta\theta/\Delta t$. We approximate the flow around the droplet by the equations for Stokes flow, which is a reasonable approximation for the size range of droplets in the troposphere considered in these calculations.

The equations for Stokes flow can be obtained, for example, from Pruppacher and Klett [1997, Eqs. (10.12) and (10.36)], and when expressed in terms of the normalized radius r yield

$$u_r = -U_\infty \cos\theta \left(1 - \frac{3}{2r} + \frac{1}{2r^3} \right), \quad (5)$$

$$u_\theta = U_\infty \sin\theta \left(1 - \frac{3}{4r} - \frac{1}{4r^3} \right). \quad (6)$$

The electrical force F produces a radial velocity u_e relative to the flow, where $u_e = BF$, with B being the mobility of the particle, which depends on its radius and the viscosity of the air. Combining Stokes flow with the effect of the electrical force (no Brownian or inertial or phoretic effects) we have

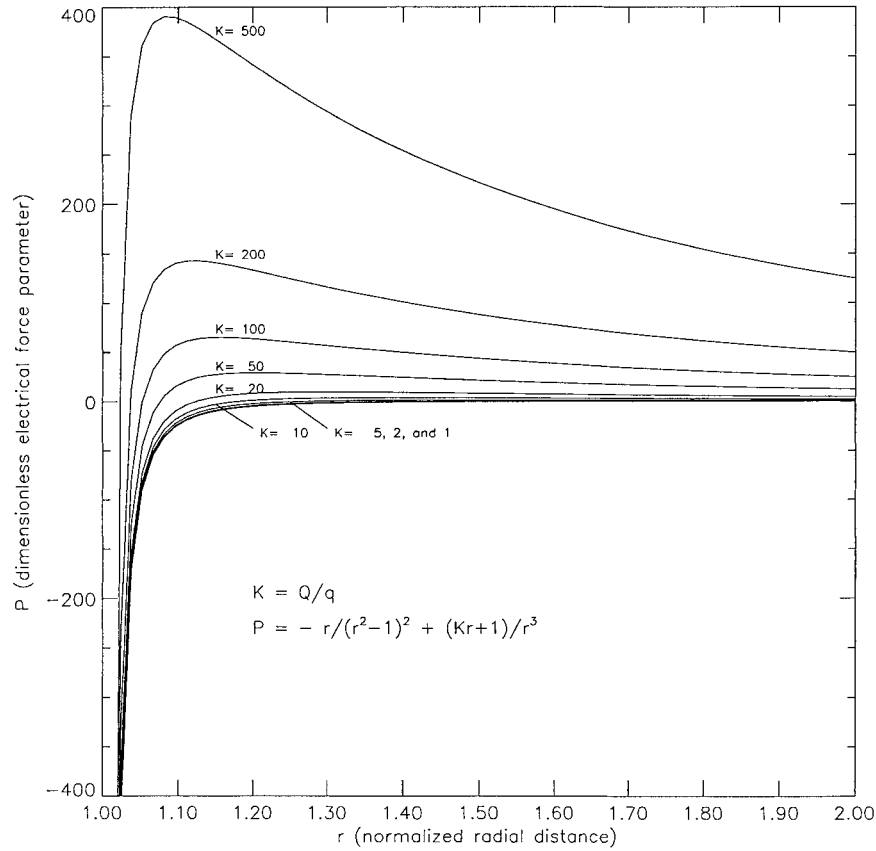


FIG. 2. The variations, with normalized radial distance r from the droplet, of the force parameter P for various values of the ratio K of the droplet to aerosol charge when the droplet and aerosol particle have charges of the same sign.

$$\Delta r = -U_\infty \cos\theta \left(1 - \frac{3}{2r} + \frac{1}{2r^3} \right) \Delta t + BF\Delta t, \quad (7)$$

$$\Delta \theta = U_\infty \sin\theta \left(1 - \frac{3}{4r} - \frac{1}{4r^3} \right) \frac{\Delta t}{r}, \quad (8)$$

so that with F from Eq. (4)

$$\frac{\Delta r}{\Delta \theta} = -\frac{r}{\tan\theta} \left(1 - \frac{3}{2r} + \frac{1}{2r^3} \right) \left(1 - \frac{3}{4r} - \frac{1}{4r^3} \right)^{-1} + \frac{BCP}{U_\infty} \left[\frac{\sin\theta}{r} \left(1 - \frac{3}{4r} - \frac{1}{4r^3} \right) \right]^{-1}, \quad (9)$$

where

$$P = -\frac{r}{(r^2 - 1)^2} + \frac{1}{r^3}(Kr + 1). \quad (10)$$

Thus the calculations of aerosol particle trajectories need only be made for values of two variables: the lumped constant BC/U_∞ and the variable $K = Q/q$. If we had considered the aerosol particles as being represented by spheres rather than points, the equations

become considerably more complex (Grover and Beard 1975) and the numerical integrations must be made for more than the above two variables. It can be shown that instead of point charges, the charge of the aerosol and its image would be represented by small line charges, and the forces between them would be represented by the forces between monopole, dipole, quadrupole, and higher-order moments. For increasing aerosol particle size the dipole moments are the next that need to be considered and the orientation of the dipoles is such as to increase the attraction due to the monopoles. So the present results provide a lower limit to the attractive force.

3. Results of numerical integrations for collision efficiency

Figure 2 shows the variation of the parameter P as a function of r for various positive values of K (i.e., same sign of charge on droplet and particle). At large distances the second term on the right-hand side of Eq. (10) dominates, representing Coulombic repulsion, but there is a transition to image charge attraction at a nor-

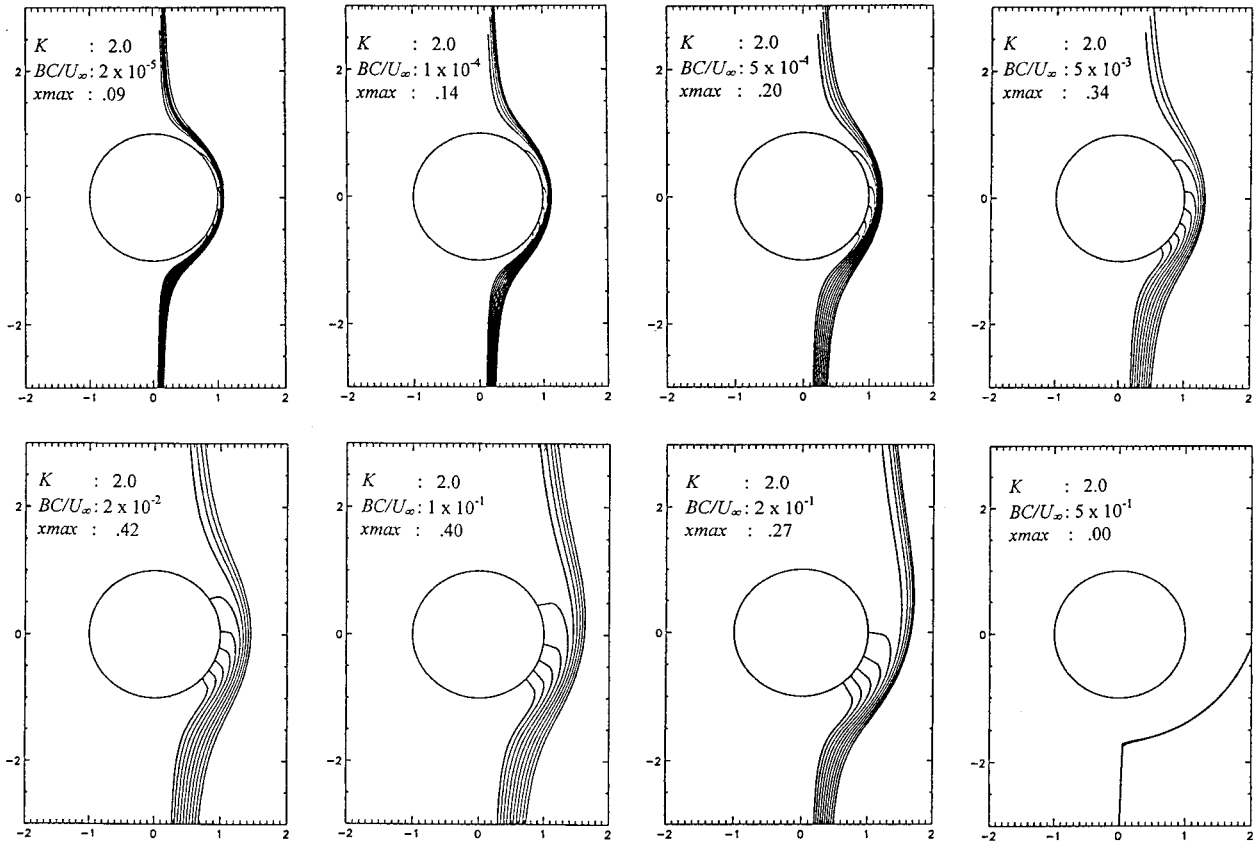


FIG. 3. A sample of trajectory calculations similar to those utilized, for like droplet and particle charges, with $K = 2$ and various values of the parameter BC/U_∞ . The value of x_{max} , representing the maximum offset from the axis of symmetry for which the particle collides with the droplet, increases up to a maximum as BC/U_∞ increases, then it decreases to zero. The increase is due to the increasing strength of the attractive force. This subsequent decrease of x_{max} with increasing BC/U_∞ is due to the electrical repulsive force becoming large enough to prevent the particle being carried toward the droplet by the flow, so that it is diverted around it instead of getting to a point close enough so that the repulsive force is overcome by the attractive force.

malized distance that depends on K . For K values of 500, 100, 20, 5, and 1 the change from repulsion (P positive) to attraction (P negative) is at values of r of 1.02, 1.05, 1.12, 1.26, and 1.62. Thus, for equal and same sign charges on the droplet and particle, the image charge force dominates for the particle as far away from the droplet surface as 60% of the radius of the droplet. The air flows relative to the droplet at a speed whose asymptotic value is U_∞ and carries the charged particle towards the droplet against the repulsion. If K and the lumped parameter BC/U_∞ are not so large that the particle is repulsed as fast as the radial component of the flow carries it towards the droplet, then the particle will pass through the radial distance of maximum repulsion, and then in most cases it will pass through the transition to attraction and collide with the droplet, as the image forces increase very rapidly as r tends to 1.

Equation (9) was integrated numerically with a standard numerical integration package on a VAX 4000/500 computer, for K values of 0, ± 1 , ± 2 , ± 5 , ± 10 , etc., to ± 1000 , in combination with BC/U_∞ values of 2×10^{-9} ,

5×10^{-9} , 1×10^{-8} , 2×10^{-8} , etc., to 2×10^1 . Fig. 3 shows a sample of calculated trajectories similar to those utilized for like charges on droplets and aerosols and BC/U_∞ ranging from 2×10^{-6} to 7×10^{-1} . For each combination of K and BC/U_∞ a family of trajectories was calculated, with increasing offset x from the axis of symmetry, as illustrated. There is a maximum initial offset x_{max} for which an aerosol collision with the sphere will occur, that is, the trajectory with x equal to x_{max} is a trajectory that crosses $r = 1$, and the trajectory with x greater than x_{max} passes by. The initial placement of the aerosol particle was offset horizontally from the vertical axis through the center of the droplet at a distance of six radii below the droplet center although Fig. 3 (to save space) only shows the trajectory from three radii below.

For small BC/U_∞ and small K there will always be a capture for a small x , that is, the electrostatic repulsion force does not produce a vertical component of drift velocity as large as U_∞ . The value of x_{max} initially increases with BC/U_∞ as the electrically induced velocity

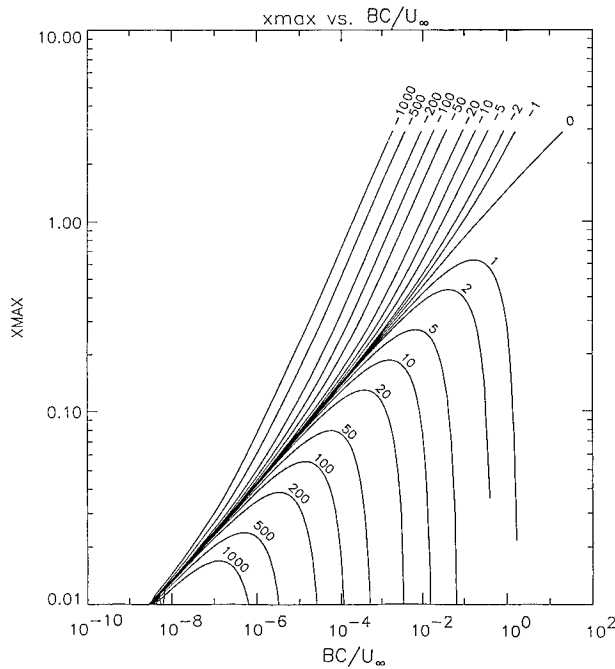


FIG. 4. Variation of x_{\max} with BC/U_{∞} , for positive, zero, and negative values of K , the ratio of droplet to particle charge. Each curve in the family is labeled by its value of K . The collision efficiency is equal to x_{\max}^2 .

increases relative to U_{∞} , provided that the particle is able to pass through the distance of maximum repulsion. As BC/U_{∞} continues to increase this is no longer true, and in Fig. 3 for $K = 2$ and $BC/U_{\infty} = 5 \times 10^{-1}$ the repulsive force is great enough to prevent collisions for any x .

Figure 4 is a plot of x_{\max} values versus BC/U_{∞} in the form of a family of curves for different values of K . For small BC/U_{∞} the x_{\max} values remain constant or change only very slowly with K , that is, the net charge on the droplet has little effect. For larger BC/U_{∞} with positive K the values of x_{\max} become zero with repulsion preventing close approach, as discussed earlier. For larger BC/U_{∞} values and increasingly negative K , the values of x_{\max} continue to increase.

Given that the collision efficiency E is the ratio of the initial volume occupied by those aerosol particles that collide in a time interval of say Δt compared to the volume swept out by the falling droplet in the same time interval, the collision efficiency is just

$$E = \pi x_{\max}^2 U_{\infty} \Delta t / [\pi (1.0)^2 U_{\infty} \Delta t] = x_{\max}^2. \quad (11)$$

Figures 5–8 contain plots of collision efficiency x_{\max}^2 as a function of aerosol radius, which we denote a , for a given droplet radius A and net charge Q . A family of curves is given in each case covering different values of aerosol particle charge q . (The values of Q and q on the figures are in terms of elementary charges e , where $e = 1.602 \times 10^{-19}$ Coulombs.) The family of curves corresponds to the family of K values selected previ-

ously with Q determining q in each case, which together with a and A determine the BC/U_{∞} values used to obtain the required x_{\max} value. This x_{\max} value is an interpolation of the array of x_{\max} values obtained from the numerical integrations from which Fig. 4 was derived.

The value of the mobility B as a function of particle radius a is given by

$$B = (1 + \alpha N_{\text{Kn}}) / (6\pi\eta_a a), \quad (12)$$

where N_{Kn} is the Knudsen number, which is the ratio of the mean free path of air molecules to the radius of the particle, α is a slowly varying constant of order unity (Pruppacher and Klett 1997, section 11.3), and η_a is the dynamic viscosity coefficient of air that we take as being $1.68 \times 10^{-5} \text{ kg m s}^{-1}$ to represent midtropospheric air. For a particle of radius $0.1 \mu\text{m}$ the value of B used was $8.67 \times 10^{10} \text{ kg}^{-1}\text{s}$. The values of U_{∞} as a function of droplet radius are taken from the curves of Pruppacher and Klett (1997, section 10.3.6) as appropriate for droplets falling in air of density and temperature of the midtroposphere. All of the families of curves for positive K (i.e., for droplet and particles with charges of the same sign) are similar and can be transformed to match each other for a given K value by appropriate displacements along the horizontal axis. The same is true for the families of curves for zero K and for negative K . The displacements are nonuniform in a .

The curves of Fig. 5 are for droplets of $42\text{-}\mu\text{m}$ radius and include some of the results from Wang et al. (1978). In Fig. 5a the heavy solid and dashed curves are for collision efficiencies in the absence of electrical effects for RH of 100%, 95%, and 75%. The charges on the droplet and particles were of opposite sign and proportional to the square of their radii, so that the particle charge varies along the length of the two light lines, which are for the electrically enhanced collision rates at 95% and 75% RH, with a charge of $-73\ 400e$ on the droplet. The continuous lines change to dashed lines when inertial effects are included and Brownian motion is neglected. The charges on the aerosol particles range from less than $1e$ up to $42e$, between 0.1- and $1.0\text{-}\mu\text{m}$ radius. Implications were drawn, from the enormous charge required on the droplet for a significant increase in collision efficiency, that electrical effects on droplet–aerosol particle collisions would be insignificant except in thunderclouds.

Figures 5b, 5c, and 5d show the collision efficiencies from the present calculations, with zero droplet charge in 5b, and $+500e$ and $-500e$ in 5c and 5d. The particle charges range from 5 to $500e$. The curves for the absence of electrical effects at 100% and 95% RH are included for comparison. These RH values are representative of an environment that is at or above ice saturation for a temperature less than -5°C . The results demonstrate that when image charges are considered it is possible to obtain more than one order of magnitude increase in collision efficiency with only $100e$ on the aerosol particles, and this applies for aerosols of radii

0.1–1.0 μm even when there is a charge of the same sign of as much as $500e$ on the droplet.

In Fig. 5b (zero droplet charge) the circled points are from Grover and Beard (1975) and are in reasonable agreement with the present results. The small differences could be due to the use of midtropospheric temperatures and pressures and the Stokes flow approximation in the present calculations.

A comparison of Figs. 5b, 5c, and 5d indicates that varying the droplet charge from $-500e$ to $+500e$ has significant effects only for aerosol particles smaller than about 0.1 μm . For the larger particles almost all of the increase in collision efficiency is due to image charges and the effect of the droplet charge Q is minor. For the smaller particles a same-sign change on the droplet reduces the collision efficiency, which goes to zero if $Q = +500e$ and the particle size is less than 0.01 μm , as shown in Fig. 5c. For opposite-sign changes on the droplet, the collision efficiencies are markedly increased for the smaller aerosol particles, as shown in Fig. 5d.

Figure 6 shows results in the same format for droplets of radius 30 μm and charges of zero, $+500e$, $-500e$, and $+100e$. In the latter case the range of particle charges was from $1e$ to $100e$. From a comparison of Figs. 5b, 5c, and 5d on the one hand with Figs. 6a, 6b, and 6c on the other we can see the effects of droplet size on collision efficiency for a given charge (say $100e$) on the aerosol particle. Confining ourselves for simplicity to considering the larger-sized particles, the effect of a smaller droplet (smaller U_∞ at constant B and C) is a larger absolute collision efficiency. The increase for the 30- μm droplets as compared to that for the 42- μm droplets is about 30%. In terms of Fig. 4, a smaller U_∞ implies a larger BC/U_∞ and a larger x_{max} in the region of independence of K . It should be noted however, that when the relative change in collision efficiency over values for uncharged aerosol particles (heavy curves) is considered, rather than the change in absolute collision efficiency, the decrease in droplet size produces about a 30% decrease in the relative collision efficiency.

The effect of the decrease in droplet charge on the aerosol particle radius at which maximum collision efficiency occurs (for like charges on droplet and particle) is illustrated by a comparison of Figs. 6b and 6d. The peak in x_{max}^2 moves to smaller values of a with the reduction in Q .

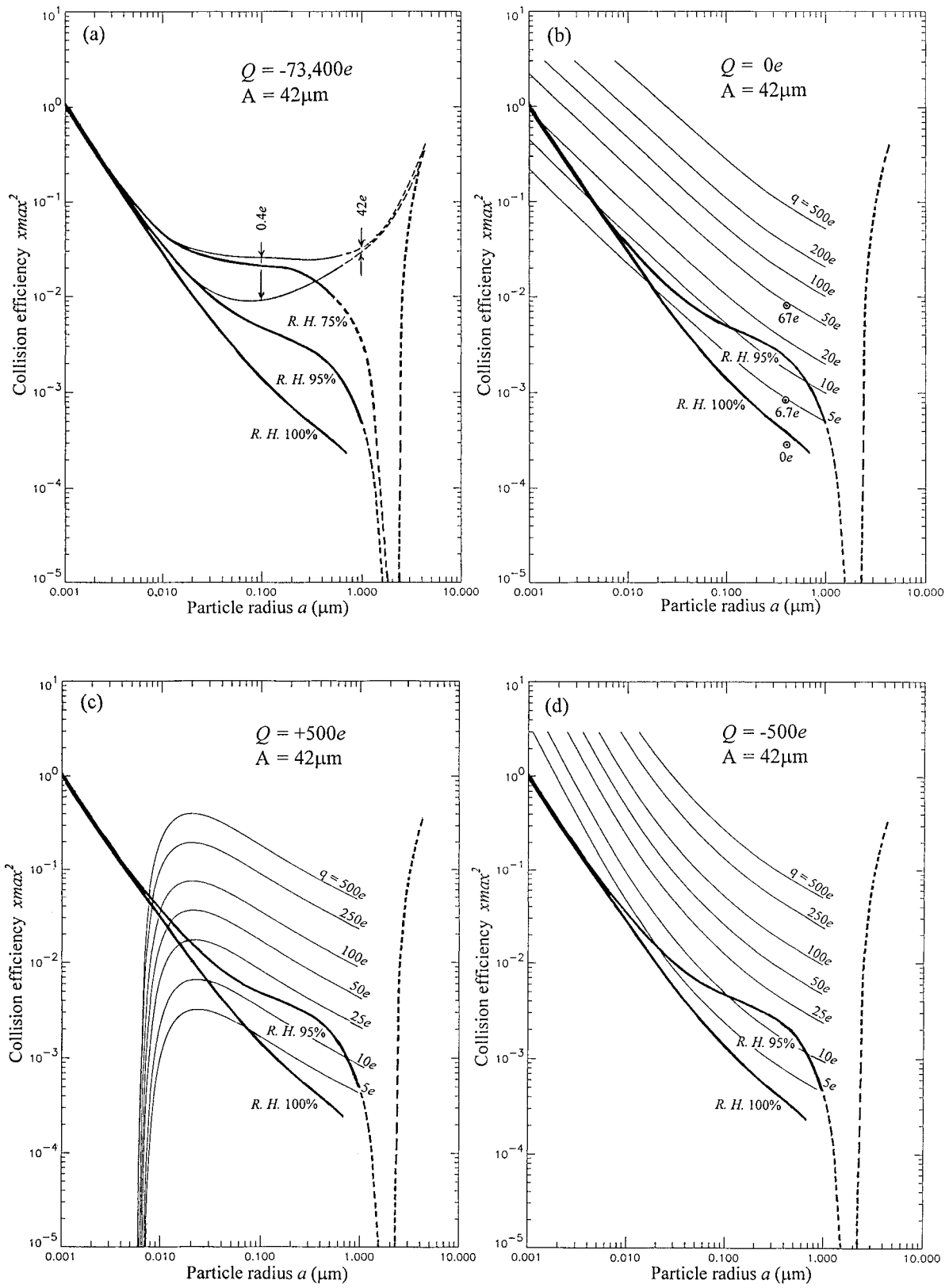
Figures 7, 8, and 9 show results in the same format as Fig. 6 for droplets of radii 18.6, 72, and 106 μm . As expected from the previous result, the trend for smaller

absolute collision efficiencies with increasing droplet size is confirmed over the whole range of droplet radius from 18.6 to 106 μm . But again, when the relative change in collision efficiency over values for uncharged aerosol particles is considered, an increase in droplet size produces an increase in the relative collision efficiencies.

A droplet falling through a population of charged aerosol particles will continuously collect particles and their charge until it has accumulated so much charge that the long range repulsion force prevents more collection. It is possible to evaluate the maximum charge collected by considering the artificial situation where the aerosol particles are all of the same size and charge. This leads to a result that has implications for the more general atmospheric situation, as we will see. It is relevant to cloud conditions such as in a downdraft where a population of charged droplets is evaporating to maintain near 100% RH. The evaporation of the smaller charged droplets down to haze particles, or in some cases to dry aerosols, brings their fall velocity to zero and facilitates their capture by image charge forces as the larger droplets continue to fall through them. One consequence of such a situation is that if the falling droplets are supercooled, some of the aerosol particles they collide with are likely to be active as ice forming nuclei, and freezing of the droplets could result, as we will discuss later. Another consequence is that the droplet will collect the charge of the particles it collides with. The maximum charge that a falling droplet will collect can be inferred from Table 1, which contains an array of x_{max} values for positive K , arranged according to values of BC/U_∞ and K . Consider a droplet of radius A with some small or zero initial charge. The droplet radius and the radius of the aerosol particles and the charge q that is on them together determine the value of BC/U_∞ . The initial value of K is small, and it increases each time a collision occurs and a particle and its charge are collected as the droplet descends. The values of BC/U_∞ remain essentially constant with K increasing, so that the situation is equivalent to starting with a value of K and x_{max} near the bottom of the table and ascending a column in the table with increasing K . (The droplet radius increases as particles are collected, but only very slightly.) The maximum charge that can be collected by the descending droplet before the collision efficiency goes to zero is defined by K_{max} , which is the value of K for which x_{max} goes to zero on ascending the column.

→

FIG. 5. Collision efficiency x_{max}^2 for aerosol particles of radius a with droplets of radius $A = 42 \mu\text{m}$ and charge Q . The heavy solid curves are from Wang et al. (1978) for Brownian and phoretic effects, and the dashed curves are for phoretic and inertial effects, with RH as indicated. For (a) the light curves are the results of Wang et al. (1978) for the sum of the electrical and other effects, with particle charges varying as a^2 , of magnitude $0.4e$ for $a = 0.1 \mu\text{m}$, and $42e$ for $a = 1.0 \mu\text{m}$. The droplet charge is of opposite sign to that of the particles and is $-73\ 400e$. For (b), (c), and (d) the light curves are the present calculations for electrical effects only, with the family of curves for particle charges q independent of a and ranging from 5 to $500e$ as designated. The droplet charge is zero, $+500e$, and $-500e$ in (b), (c), and (d). The circled points in (b) are for the image charge calculations of Grover and Beard (1975).



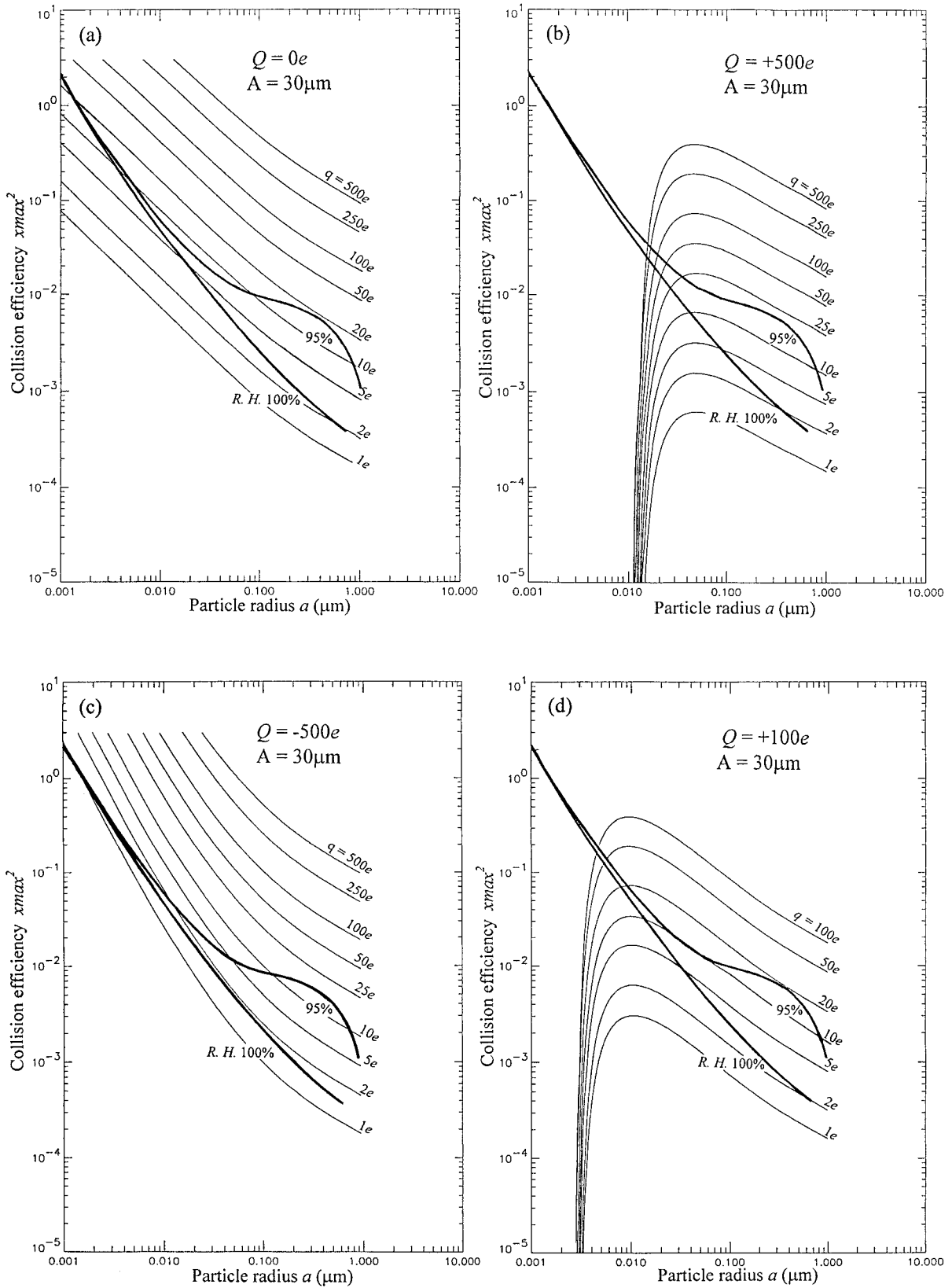


FIG. 6. Collision efficiency x_{max}^2 for aerosol particles of radius a with droplets of radius $A = 30 \mu\text{m}$ and charge Q . The heavy solid curves are from Wang et al. (1978) for Brownian and phoretic effects with RH as indicated. The families of light curves are the present calculations for electrical effects only. For (a), (b), and (c) the light curves represent droplet charges of zero, +500, and -500e, respectively, and particle charges of 1e-500e. For (d) the light curves represent a droplet charge of +100e and particle charges of 1-100e.

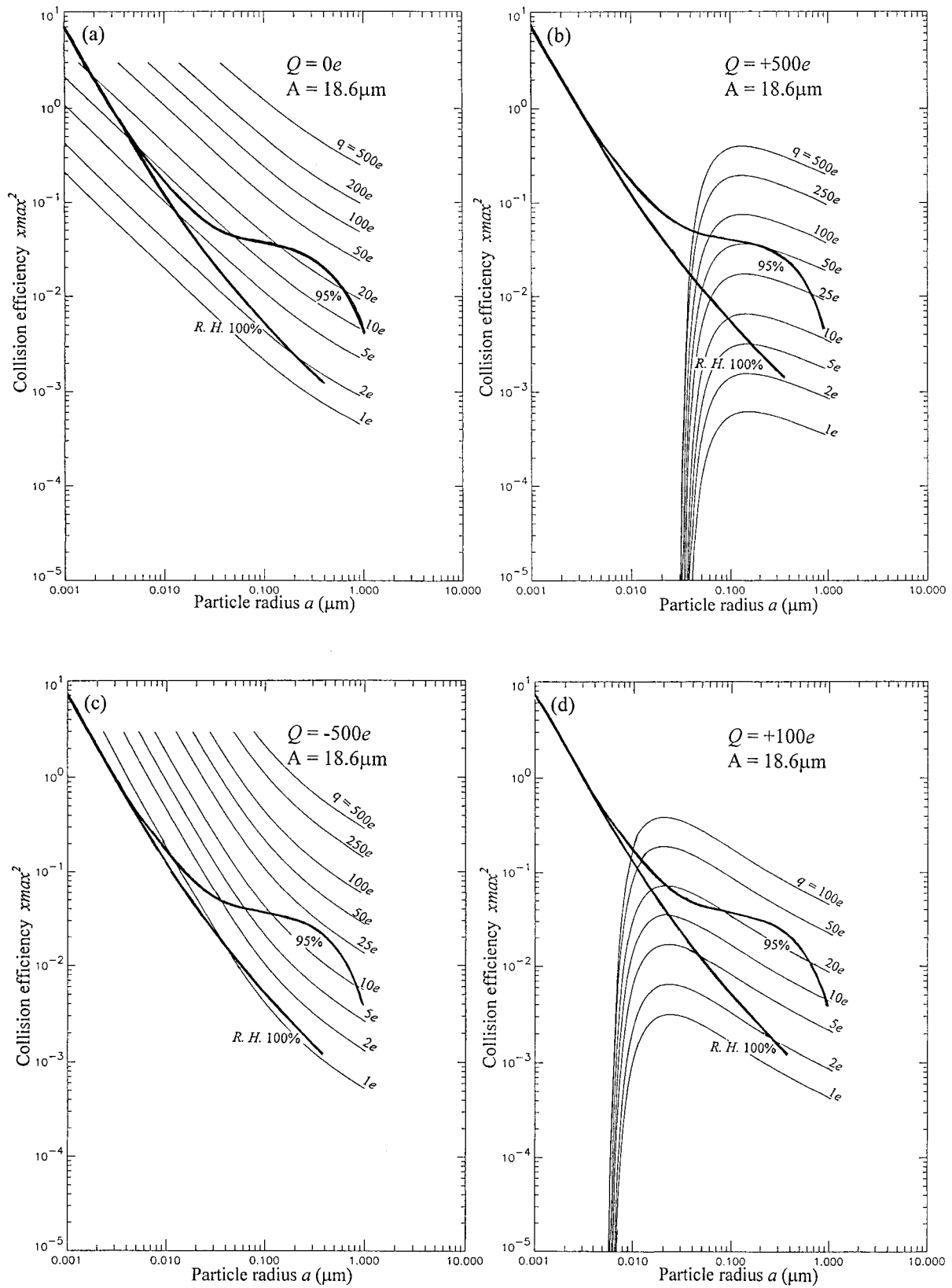


FIG. 7. Collision efficiency x_{\max}^2 for particles of radius a with droplets of radius $A = 18.6 \mu\text{m}$ and other parameters as in Fig. 6.

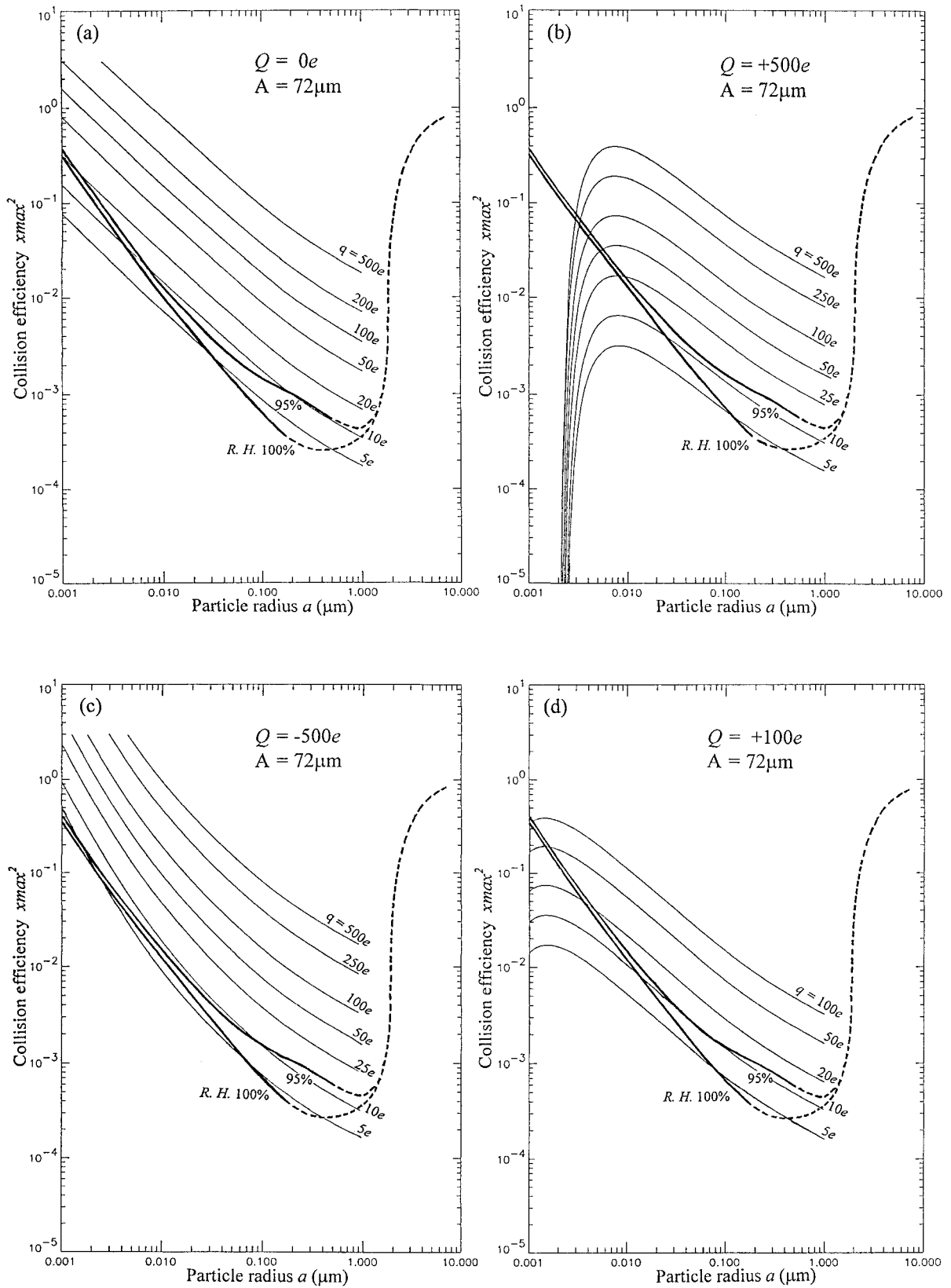


FIG. 8. Collision efficiency x_{max}^2 for particles of radius a with droplets of radius $A = 72 \mu\text{m}$ and other parameters as in Fig. 6.

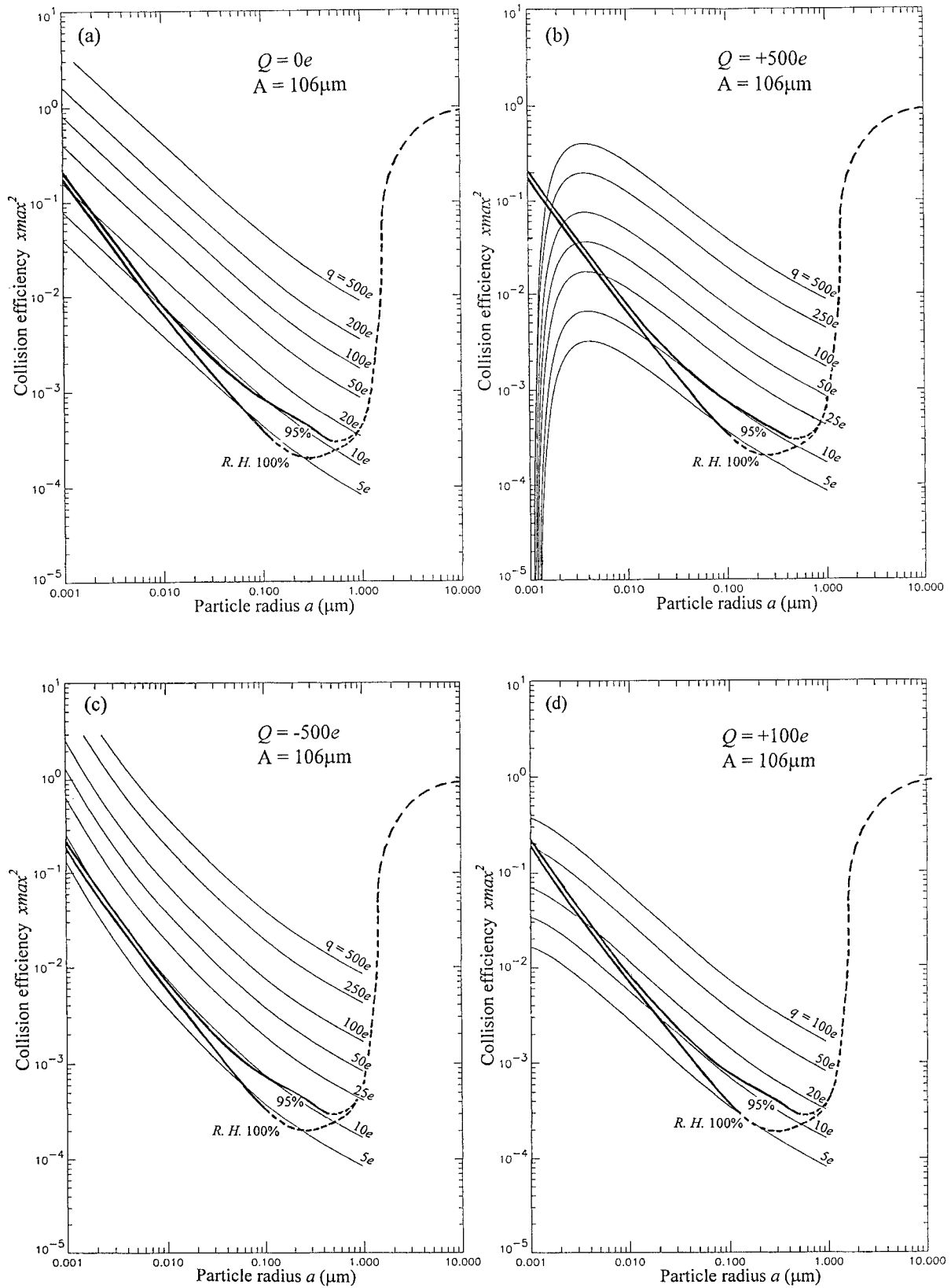


FIG. 9. Collision efficiency x_{\max}^2 for particles of radius a with droplets of radius $A = 106 \mu\text{m}$ and other parameters as in Fig. 6.

TABLE 1. The selected values of x_{\max} for various BC/U_∞ and K values to show the maximum value of K that can be gained by collision with charged aerosol particles. When the particle charges are all the same this is equivalent to estimating the maximum charge that can be gained by the droplet. Fixing the value of droplet radius fixes the value of U_∞ , and then there are combinations of values of aerosol particle radius and charge that apply to each column designated by a BC/U_∞ value in the table.

BC/U_∞	2×10^{-6}	1×10^{-5}	5×10^{-5}	2×10^{-4}	1×10^{-3}	5×10^{-3}	2×10^{-2}	1×10^{-1}	5×10^{-1}	2×10^0
K	x_{\max} as a function of BC/U_∞ and K									
1000	0									
500	0.02	0								
200	0.04	0.03	0							
100	0.04	0.05	0.04	0						
50	0.05	0.07	0.08	0.06	0					
20	0.05	0.07	0.10	0.12	0.11	0				
10	0.05	0.07	0.11	0.15	0.18	0.15	0			
5	0.05	0.08	0.11	0.16	0.22	0.27	0.22	0		
2	0.05	0.08	0.11	0.16	0.24	0.34	0.42	0.40	0	
1	0.05	0.08	0.12	0.16	0.25	0.36	0.48	0.61	0.52	0
$(BC/U_\infty)K_{\max}^2$	2	2.5	2	2	2.5	2	2	2.5	2	2

Thus, the descending droplet charges up to a maximum charge of $Q_{\max} = qK_{\max}$.

The range of BC/U_∞ values in the table for a given droplet radius and particle radius corresponds to different charges on the particle. The set of zeros running as a diagonal through the table suggest a power-law relationship between K_{\max} and BC/U_∞ . The row of numbers at the bottom of the table gives the product $(BC/U_\infty)K_{\max}^2$ and it can be seen to be approximately constant. (The lack of smooth variation is due to the finite step size in K .) The approximate constancy of the product can be fitted to an approximate relationship $K_{\max} \approx 1.5(BC/U_\infty)^{-1/2}$. Substituting for C we have

$$Q_{\max} \approx 1.5q(4\pi\epsilon_0 A^2/q^2)^{1/2}(B/U_\infty)^{-1/2}, \tag{13}$$

$$Q_{\max} \approx 1.5(4\pi\epsilon_0 U_\infty/B)^{1/2}A. \tag{14}$$

Thus we find Q to be approximately independent of the charge on the aerosol particles. The expression for maximum charge is thus appropriate when there is a distribution of charge on aerosol particles in a field, provided that they are monodispersive in size. Also, U_∞ varies approximately as A^2 (Pruppacher and Klett 1997, section 10.3.6) so that Q_{\max} varies approximately as A^2 . As examples of Q_{\max} values from this formula, we consider a 42- μm radius droplet and particles of radii 1 and 0.1 μm , respectively. The maximum charge accumulated by this droplet is then 30 000 and 6000 e , respectively. For a 72- μm droplet with particles of radii of 1 and 0.1 μm the maximum charges are 50 000 and 10 000 e .

While the situation in the real atmosphere is considerably more complicated, it does appear that the capture of charged particles by a descending droplet represents a droplet charging mechanism not hitherto recognized.

4. Lifetime of the charge on aerosol particles

The importance of these electrical effects in clouds will depend directly on the time available for interaction before the charge “leaks away” from the aerosol par-

ticle. The loss of charge by breakdown ionization of air is unimportant for particles in the size and charge range of interest here, because the electric field near the particle diverges rapidly, in a distance small compared to that needed to initiate an electron avalanche.

The most important process for loss of charge is collisions with, and capture of, air ions with charge of opposite sign. The rate of neutralization of particle charge by capture of air ions depends on their concentration and their mobility. The major source of air ions above the lowest 1 or 2 km in the atmosphere is cosmic ray ion pair production. The initial positive and negative ions immediately attach to air molecules, which in turn attach to water molecules, with the size of the clusters dependent on the RH. For clear dry air the concentration and mobility of the air ions are fairly well known, but for hazy and cloudy air both parameters are reduced to a large and variable extent by the water vapor, haze particles, and droplets. The ions attach to haze particles and to water droplets, and mutual neutralization of positive and negative ions can occur on them. A large decrease in conductivity occurs in clouds and has been found in layers of haze for which the RH is approaching 100% (Reiter 1992, section 4.2.2.1). Also, Dolezalek (1963) and Anderson and Trent (1966) and others have found a decrease in the conductivity of apparently clear air before fog formation. Additional considerations are the initial amount of charge on the droplet before evaporation, which will depend on the charging process, and which is likely to involve the presence of excess charge of one sign (space charge) in a volume of air. Some of the excess charge may persist after the droplets have evaporated, further slowing the rate of loss of charge from the aerosol particle. We will now discuss factors influencing the lifetime against loss of charge for particles in clear dry air in the midtroposphere, leading to an estimate of the values in cloudy air.

The equations relevant to charging and discharging aerosol particles by air ions are given in Pruppacher and

TABLE 2. Values of the right-hand side of Eq. (22) that scale the initial lifetime of charge, on charged aerosol particles of radii a ranging from 0.01 to 1.00 μm and with charge ranging from 1 to 500 elementary charges, with other parameters as in the text. The negative values represent conditions for a particle to gain charge rather than lose it. The diagonal separating the positive and negative values represents charge equilibrium with the lifetime tending to $\pm\infty$.

a (μm)	q (e)								
	1	2	5	10	20	50	100	200	500
0.01	1.01	1.00	1.00	1.00	1.00	1.00	1.00	1.00	1.00
0.02	1.34	1.01	1.00	1.00	1.00	1.00	1.00	1.00	1.00
0.04	-1.84	1.34	1.00	1.00	1.00	1.00	1.00	1.00	1.00
0.10	-0.17	-0.74	1.34	1.01	1.00	1.00	1.00	1.00	1.00
0.20	-0.06	-0.17	-1.84	1.34	1.01	1.00	1.00	1.00	1.00
0.40	-0.03	-0.06	-0.25	-1.84	1.34	1.00	1.00	1.00	1.00
1.00	-0.01	-0.02	-0.06	-0.17	-0.74	1.34	1.01	1.00	1.00

Klett (1997) in sections 18.1 and 18.2. They lead to the following expressions for the case of a positively charged particle, with charge q_a and radius a , experiencing collisions with both positive and negative ions, with each ion singly charged. We here denote the magnitude of the elementary charge by q_e to avoid confusion with our usage in this section of e to denote the base of natural logarithms. The flux of colliding positive ions is

$$j_+ = 4\pi B_+ \frac{kT}{q_e} n_+ a \left(\frac{\tau}{e^\tau - 1} \right) \quad (15)$$

elementary charges per second and the flux of colliding negative ions is

$$j_- = 4\pi B_- \frac{kT}{q_e} n_- a \left(\frac{\tau}{1 - e^{-\tau}} \right) \quad (16)$$

elementary charges per second where

$$\tau = \frac{q_a q_e}{4\pi \epsilon_0 k T a} \quad (17)$$

with q_a and q_e in SI units, and where n_+ and n_- are the concentrations of positive and negative ions far from the aerosol; B_+ and B_- are the mobilities of the positive and negative ions, and T is the absolute temperature. The parameter τ depends on the ratio of the electrical potential of the ions at the particle surface to their thermal energy. The decay of charge is approximately exponential when the charge is far from its equilibrium value with an initial lifetime L against decay given by

$$L = q_a / (q_e j_+ - q_e j_-) \quad (18)$$

so that

$$\frac{1}{L} = \frac{q_e}{\epsilon_0} \{ B_- n_- (1 - e^{-\tau})^{-1} - B_+ n_+ (e^\tau - 1)^{-1} \}. \quad (19)$$

For τ large compared to 1 (larger q_a and/or smaller a) the term $(1 - e^{-\tau})^{-1}$ tends to 1 and the term $(e^\tau - 1)^{-1}$ is small, so that the magnitude of j_- is large compared to that of j_+ and

$$L \sim \epsilon_0 / \sigma_-, \quad (20)$$

where σ_- is the negative conductivity, given by

$$\sigma_- = q_e B_- n_-. \quad (21)$$

For τ not large compared to 1 (smaller q_a and/or larger a) the decay is no longer quasi-exponential; the thermal velocity of the ions becomes important and also j_+ tends to restore positive charge to the particle. Given enough time, an equilibrium will be reached with $j_+ = j_-$ and with the magnitudes of the two terms within the curly brackets on the right-hand side of (19) being equal. In clear air B_- is 25%–40% larger than B_+ (Pruppacher and Klett 1997, section 18.1) and if $n_+ = n_-$ then τ is approximately -0.3 at equilibrium and there is on average a small negative charge on the particle. Taking $T = 256$ K and particles of radii 0.01, 0.1, and 1.0 μm the equilibrium average values of q are $-0.05q_e$, $-0.5q_e$, and $-5q_e$, respectively. However, if n_+ is considerably greater than n_- as in the cases of space charge layers in clouds to be discussed later then the equilibrium charge on the particles will remain positive and $1/L$ will go to zero before the particles have lost all their positive charge. For the same temperature and $n_+ = 10n_-$ equilibrium is attained for $\tau \sim 2.0$, so that the equilibrium average charges on particles of radii 0.01, 0.1, and 1.0 μm are $0.3q_e$, $3q_e$, and $30q_e$, respectively.

Equation (19) can be rewritten as

$$\frac{L\sigma_-}{\epsilon_0} = \left\{ (1 - e^{-\tau})^{-1} - \frac{B_+ n_+}{B_- n_-} (e^\tau - 1)^{-1} \right\}^{-1}, \quad (22)$$

which again can be seen to reduce to (20) when τ is large with the expression within the curly brackets tending to 1. In Table 2 we show the values of the right-hand side of this equation taking B_- as 36% larger than B_+ and $n_+ = 10n_-$ and a temperature of 256 K. The values in this table can be multiplied by ϵ_0/σ_- to give the initial lifetime L against loss of charge for the specific values of particle radius and charge being considered. The negative values in the table represent conditions for a particle to gain charge rather than lose it and the boundary between positive and negative values is for the Boltzman equilibrium with infinite lifetime. The effect of the image charge of the ion in the particle has

been neglected; it may have a small effect for particle radii less than $0.04 \mu\text{m}$.

When one applies this theory to an atmospheric environment, there is considerable uncertainty in determining the applicable values of atmospheric conductivity or the ion concentrations and mobilities that determine the conductivity. One environment of interest is the interface, at the tops of clouds, between cloudy and clear air, where charged droplets are evaporating. Provided the altitude is above the top of the mixing layer, the conductivity of the clear, low humidity air above the interface is fairly well determined and depends on altitude, latitude, and phase of the solar cycle (all affecting the cosmic ray flux and the ion production rate) and on the amount of volcanic aerosol present. Within the mixing layer the presence of dust and atmospheric pollutants of various kinds reduces the conductivity, while radioactive materials lifted up from the land surface increase it. These factors are reviewed by Gringel et al. (1986). As noted, the concentration of air ions and the conductivity within clouds are considerably reduced by the attachment of air ions to droplets and recombination of ions with those of opposite sign on the surface of droplets. (Pruppacher and Klett (1997, section 18.3) compare theory and observation and report that within clouds the conductivity is reduced by a factor of between 3 and 40. Rust and Moore (1974) found that the conductivity of cloudy air was 10% that of clear air at the same altitude. Thus to estimate a value for σ_- to use when applying the results of Table 2 to clouds we take the representative value of $\sigma_- = 10 \times 10^{-14} \Omega^{-1}\text{m}^{-1}$ at 5-km altitude (Gringel et al. 1986) and reduce it by a factor of 10 for cloudy air. For the limiting case of large aerosol particle charge and small radius and with the above conductivity we find the lifetime $L = 10^{14} \epsilon_0$, which is about 15 min. Table 2 provides scaling factors for aerosols with smaller charge and larger radii.

5. Implications of electroscavenging of evaporation nuclei

a. Production of highly charged evaporation aerosols

At the tops of clouds the interface region between the cloudy and clear air has been found to develop a positive space charge, especially for stratus or stratocumulus clouds (Reiter 1992, section 4.2.2.2; Pruppacher and Klett 1997, section 18.4.1; MacGorman and Rust 1998, chapter 2). A layer of negative space charge is often found at cloud base. One of the authors (KB) is evaluating charges on cloud droplets from 1997–98 aircraft observations during the Lake-ICE (Lake-Induced Convection Experiment) project. Preliminary data indicate positive charges in cloud-top turrets (Ochs et al. 1998) and negative charges of $100e$ and greater within convective elements of a stratocumulus cloud deck. The presence of these space charge layers can be understood

as a consequence of the gradients of conductivity at the cloud boundaries interacting with the current density (J_z), which flows between the ionosphere and the surface (Tinsley 1996; MacGorman and Rust 1998).

In the idealized case of horizontal stratification the application of the Poisson equation $\nabla^2\phi = -\rho/\epsilon_0$, where ϕ is the electrical potential and ρ is the space charge density, leads to the relation $\rho = -\epsilon_0 J_z(d/dz)(1/\sigma)$. An illustration in terms of space charge in the measured conductivity gradient at the top of the mixing layer is given by Sagalyn and Faucher (1956). The limiting case of conductivity going to zero in an ideal horizontally stratified layer results in positive space charge accumulating above it and negative space charge below it, so that in $\sim 10^3$ s (the time constant of the ionosphere–earth as a plane-parallel capacitor) the full 250 kV of ionosphere–earth potential difference would appear across the layer of zero conductivity. But in real clouds this limit is not reached, even if the conductivity was effectively zero, because of the transport of charge by turbulence and the finite horizontal extent of the cloud.

For nonthunderstorm warm clouds charges of up to several hundred elementary charges are measured on droplets of radius $25\text{--}40 \mu\text{m}$ (Pruppacher and Klett, Fig. 18-1). The process by which the space charge is transferred from ions and aerosol particles to droplets may include drift charging and other processes not well understood (including that suggested at the end of section 3, when repeated cycles of evaporation and collection in downdrafts are occurring, as in weak turbulence). Whatever the charging mechanism, the droplets with charges up to several hundred elementary charges will be subject to evaporation in downdrafts. At cloud top mixing with dry air (which may contain space charge) can occur with evaporation proceeding down to dry aerosol particles. Further mixing then brings these into the cloud in microscale dry layers and larger droplets fall into these.

Little charge is lost from droplets by the evaporation process (Robertson 1969) resulting in a population of highly charged evaporation nuclei (Beard 1992), which are then subject to a slow loss of charge with lifetime L as discussed. It is apparent from the present calculations that the action of image charges ensures that electrical effects dominate collision rates of these evaporation nuclei with other droplets, with as little as a few tens of elementary charges on the aerosols.

b. Evaporation aerosols as ice nuclei

Aerosol resulting from evaporation of cloud droplets have surface properties that enhance ice nucleation, such as soluble surface impurities (see Beard 1992) and insoluble organic compounds previously scavenged from the air (Garrett 1978). As previously noted, evaporation nuclei have been found to be considerably more effective as ice forming nuclei than aerosol particles that have

not been processed through clouds (Rosinski and Morgan 1991; Beard 1992; Rosinski 1995). The processes described above produce charged evaporation nuclei and enhanced collision rates, and when the cloud droplets are supercooled they may result in significant amounts of ice nucleation.

It is beyond the scope of this paper to attempt quantitative evaluation of ice nucleation rates in the atmosphere via the processes described above, but it seems possible that the rate could be high enough to be the dominant initial ice nucleation process in many clouds. At present we are unable to compare it with possible alternative processes, for example, the cooling enhancement of ice nucleation for evaporating droplets suggested by Cooper (1995).

Much could be learned from laboratory measurements of freezing rates for collisions of charged evaporation nuclei with suspended supercooled droplets. Also, it is desirable to extend the present calculations to include Brownian, phoretic, and inertial effects simultaneously with the electrical effects, and to include the effects of the finite size and mass of the evaporation nuclei.

The uncertainties could be greatly reduced by atmospheric in situ measurements of droplet size and charge distributions, aerosol particle size and charge distributions, ice crystal concentrations, small ion concentrations and mobilities, electric fields and conductivity. Measurements to quantify mixing rates would also be valuable. Measurements should be focused on weakly electrified clouds and in clouds where ice is just beginning to form.

6. Conclusions

We have calculated the effect of electrostatic charge on aerosol particles on their collision efficiencies with droplets. Such charged aerosol particles are formed from evaporating charged droplets in space charge layers at the tops of clouds. The image charge forces produce a large increase in the collision efficiency compared to that for uncharged particles, even in cases where there is a droplet charge of the same sign and magnitude as on the aerosol particles. The results are contrary to the general assumption that for nonthunderstorm clouds any electrical effects on cloud microphysics are unimportant. Thus, scavenging rates for charged evaporation aerosols are considerably enhanced, and this also constitutes a previously unrecognized droplet charging process.

The results also suggest that contact ice nucleation processes will be enhanced, especially since evaporation aerosol particles are considered to be good ice-forming nuclei, but a number of uncertainties preclude an accurate evaluation of ice nucleation rates at present. The results are relevant to the long-standing problem of ice nucleation rates in some clouds being much

higher than can be accounted for by counts of ice-forming nuclei.

Acknowledgments. This work has been supported by NSF Grants ATM 9504828 and ATM 95-05298. One of us (BAT) thanks Giles Harrison for discussions.

REFERENCES

- Anderson, R. V., and E. M. Trent, 1966: Evaluation of the use of atmospheric-electricity recordings in fog forecasting. Naval Research Laboratory Rep. 6426, 20 pp. [Available from National Technical Information Service, Sills Building, 5285 Port Royal Road, Springfield, VA 22161.]
- Beard, K. V., 1992: Ice initiation in warm-base convective clouds: An assessment of microphysical mechanisms. *Atmos. Res.*, **28**, 125–152.
- , and H. T. Ochs, 1986: Charging mechanisms in clouds and thunderstorms. *The Earths Electrical Environment*, E. P. Krider and R. G. Roble, Eds., National Academy Press, 114–130.
- Clement, C. F., and R. E. Harrison, 1992: The charging of radioactive aerosols. *J. Aerosol Sci.*, **23**, 481–504.
- Cooper, W. A., 1995: Ice formation in wave clouds: Observed enhancement during evaporation. Preprints, *Conf. on Cloud Physics*, Dallas, TX, Amer. Meteor. Soc., 147–152.
- Davis, M. H., 1969: Electrostatic field and force on a dielectric sphere near a conducting plane—A note on the application of electrostatic theory to water droplets. *Amer. J. Phys.*, **37**, 26–29.
- Dolezalek, H., 1963: The atmospheric electric fog effect. *Rev. Geophys.*, **1**, 231–282.
- Garrett, W. D., 1978: The impact of organic material on cloud and fog processes. *Pure Appl. Geophys.*, **116**, 316–334.
- Greenfield, S., 1957: Rain scavenging of radioactive particulate matter from the atmosphere. *J. Meteor.*, **14**, 115–125.
- Gringel, W., J. M. Rosen, and D. J. Hoffman, 1986: Electrical structure from 0 to 30 kilometers. *The Earths Electrical Environment*, E. P. Krider and R. G. Roble, Eds., National Academy Press, 166–182.
- Grover, S. N., and K. V. Beard, 1975: A numerical determination of the efficiency with which electrically charged cloud drops and small raindrops collide with electrically charged spherical particles of various densities. *J. Atmos. Sci.*, **32**, 2156–2165.
- Hobbs, P. V., and A. L. Rangno, 1985: Ice particle concentrations in clouds. *J. Atmos. Sci.*, **42**, 2523–2549.
- Jackson, J. D., 1975: *Classical Electrodynamics*. 2d ed. Wiley, 848 pp.
- MacGorman, D. R., and W. D. Rust, 1998: *The Electrical Nature of Storms*. Oxford University Press, 422 pp.
- Ochs, H. T., C. H. Twohy, K. V. Beard, and N. Belding, 1998: Measurements of drop and aerosol charges in and around wintertime continental clouds. Preprints, *Conf. on Cloud Physics*, Everett, WA, Amer. Meteor. Soc., 134–135.
- Pruppacher, H. R., and J. D. Klett, 1997: *Microphysics of Clouds and Precipitation*, 2d ed. Kluwer, 954 pp.
- Reiter, R., 1992: *Phenomena in Atmospheric and Environmental Electricity*. Elsevier, 541 pp.
- Robertson, J. A., 1969: Interactions between a highly charged aerosol droplet and the surrounding gas. Ph.D. dissertation, University of Illinois, 106 pp. [Available from University Microfilm, 305 N. Zeeb Rd., Ann Arbor, MI 48106.]
- Rosinski, J., 1995: Cloud condensation nuclei as a real source of ice forming nuclei in continental and marine air masses. *Atmos. Res.*, **38**, 351–359.
- , and G. Morgan, 1991: Cloud condensation nuclei as a source of ice-forming nuclei in clouds. *J. Aerosol Sci.*, **22**, 122–133.
- , D. Werle, and C. T. Naganato, 1962: Coagulation and scavenging of radioactive aerosols. *J. Colloid Interface Sci.*, **17**, 703–716.

- Rust, W. D., and C. B. Moore, 1974: Electrical conditions near the base of thunderclouds over New Mexico. *Quart. J. Roy. Meteor. Soc.*, **100**, 450–468.
- Sagalyn, R. C., and H. K. Burke, 1985: Atmospheric electricity. *Handbook of Geophysics and the Space Environment*, A. S. Jursa, Ed., Air Force Geophysics Laboratory, Bedford, Massachusetts.
- Tinsley, B. A., 1996: Correlation of atmospheric dynamics with solar wind induced changes of air-earth current density into cloud tops. *J. Geophys. Res.*, **101**, 29 701–29 714.
- Wang, P. K., S. N. Grover, and H. R. Pruppacher, 1978: On the effects of electric charge on the scavenging of aerosol particles by clouds and small raindrops. *J. Atmos. Sci.*, **35**, 1735–1743.